PERIODICA POLYTECHNICA SER. MECH. ENG. VOL. 36, NO. 1-2, PP. 23-40 (1992)

APPLICATION OF THE HYBRID-TREFFTZ FINITE ELEMENT MODEL TO THIN SHELL ANALYSIS

G. VÖRÖS

Department of Technical Mechanics
Technical University, H-1521, Budapest

Received November 5, 1991.

Abstract

The paper presents the results of a preliminary study on thin shallow shell element based on the hybrid-Trefftz (HT) model. This model adopts an assumed nonconforming displacement field which satisfies a priori the governing differential equations. The interelement continuity and the boundary conditions are enforced by frame fields defined in terms of the conventional nodal freedoms. In the p-extension, the frame functions involve an optional number of hierarchic displacement modes. Numerical results present the capability of the new shell element which can be implemented in existing finite element codes.

Keywords: hybrid finite element, thin shell.

Introduction

The hybrid-Trefftz (HT) finite element model has initially been introduced and applied for plane stress and plate bending problems in 1977 since and has been further developed [1–4]. Although the general description of the approach has already been given elsewhere [6] we start with a short and simple derivation which gives a general insight into the model. The HT method extends further the concept of assumed displacement hybrid method [7]. The variational formulation is based on the so-called hybrid-II [8] multifield functional:

$$J(\tilde{\mathbf{u}}, \mathbf{v}_e) = \sum_e J_e(\tilde{\mathbf{u}}, \mathbf{v}_e) = \sum_e \Big[\int_{\Omega_e} \frac{1}{2} \boldsymbol{\sigma}_e^T \boldsymbol{\varepsilon}_e d\Omega - \int_{\Omega_e} \overline{\mathbf{b}}^T \mathbf{v}_e d\Omega$$

$$- \int_{\Gamma_{et}} \overline{\mathbf{t}}^T \tilde{\mathbf{u}} d\Gamma - \int_{\Gamma_{eu}} \overline{\mathbf{t}}_e^T (\tilde{\mathbf{u}} - \overline{\mathbf{u}}) d\Gamma - \oint_{\Gamma_e} \mathbf{t}_e^T (\mathbf{v}_e - \tilde{\mathbf{u}}) d\Gamma \Big], \qquad (1)$$

where $\overline{\mathbf{b}}$ is the body force, Γ_{et} and Γ_{eu} are portions of the element boundary Γ_e on which either boundary tractions $\overline{\mathbf{t}}$ or displacements $\overline{\mathbf{u}}$ are prescribed. The summation extends over all elements with domains Ω_e. In

this hybrid formulation the boundary tractions $\mathbf{t}_e$, stresses $\boldsymbol{\sigma}_e$ and strains $\boldsymbol{\varepsilon}_e$ are expressed in terms of element interior displacement $\mathbf{v}_e$, while $\tilde{\mathbf{u}}$ represents the independent frame displacement field which is restricted to the Γ_e boundaries. Now, if the variation of $J(\tilde{\mathbf{u}}, \mathbf{v}_e)$ with respect to $\tilde{\mathbf{u}}$ and $\mathbf{v}_e$ is performed respectively, by virtue of the divergence theorem

$$\delta \int_{\Omega_e} \frac{1}{2} \boldsymbol{\sigma}_e^T \boldsymbol{\varepsilon}_e \, d\Omega = \oint_{\Gamma_e} \mathcal{B}^T(\mathbf{v}_e) \delta \mathbf{v}_e \, d\Gamma - \int_{\Omega_e} \frac{1}{2} \mathcal{L}^T(\mathbf{v}_e) \delta \mathbf{v}_e \, d\Omega \tag{2}$$

one obtains

$$\delta_u J = \sum_e \Big[- \int_{\Gamma_{et}} \bar{\mathbf{t}}^T \delta \tilde{\mathbf{u}} \, d\Gamma - \int_{\Gamma_{eu}} \mathbf{t}_e^T \delta \tilde{\mathbf{u}} \, d\Gamma + \oint_{\Gamma_e} \mathbf{t}_e^T \delta \tilde{\mathbf{u}} \, d\Gamma \Big] \tag{3a}$$

and

$$\delta_v J = \sum_e \Big[\int_{\Omega_e} \big(-\mathcal{L}(\mathbf{v}_e) - \bar{\mathbf{b}} \big)^T \delta \mathbf{v}_e \, d\Omega - \int_{\Gamma_{eu}} \delta \mathbf{t}_e^T \big(\tilde{\mathbf{u}} - \bar{\mathbf{u}} \big) d\Gamma$$

$$- \oint_{\Gamma_e} \delta \mathbf{t}_e^T \big(\mathbf{v}_e - \tilde{\mathbf{u}} \big) d\Gamma - \oint_{\Gamma_e} \big(\mathcal{B}(\mathbf{v}_e) - \mathbf{t}_e \big)^T \delta \mathbf{v}_e \, d\Gamma \Big] . \tag{3b}$$

According to the Trefftz approach, let

$$\mathcal{L}(\mathbf{v}_e) = \bar{\mathbf{b}} \qquad \text{and} \qquad \mathcal{B}(\mathbf{v}_e) = \mathbf{t}_e . \tag{4}$$

These conditions represent, in terms of displacement $\mathbf{v}_e$, the energy-consistent condition of internal equilibrium of an element and the proper definition of element boundary tractions. In addition to conditions (4) it is possible to impose the boundary conditions on the frame displacements, just as $\tilde{\mathbf{u}} = \bar{\mathbf{u}}$ along Γ_{eu}. Introducing these conditions to *Eqs.* (3a–b), the stationary condition $\delta J = 0$ reduces to

$$\sum_e \Big[- \int_{\Gamma_{et}} \bar{\mathbf{t}}^T \delta \tilde{\mathbf{u}} \, d\Gamma + \oint_{\Gamma_e} \mathbf{t}_e^T \delta \tilde{\mathbf{u}} \, d\Gamma \Big] = 0 , \tag{5a}$$

$$\oint_{\Gamma_e} \delta \mathbf{t}_e^T (\mathbf{v}_e - \tilde{\mathbf{u}}) \, d\Gamma = 0 , \qquad e = 1, 2, \ldots, N . \tag{5b}$$

The set (5b) indicates that the variation (3b) with respect to $\mathbf{v}_e$ must separately vanish for any element. Thus, the HT model is based on assumed displacements that a priori satisfy the governing differential equations and

enforce the interelement continuity and boundary conditions in integral sense. Such a model appears as directly opposed to the conventional displacement model in which the interelement continuity and the essential boundary conditions should be verified a priori. Different derivations which give results identical to (5a–b) were presented in references [4–5].

In the sequence for a particular element the non-conforming internal displacements or the Trefftz functions are approached by

$$\mathbf{v}_e = \dot{\mathbf{v}}_e + \sum_{j=1}^{m} N_{ej} c_{ej} = \dot{\mathbf{v}}_e + \mathbf{N}_e \mathbf{c}_e \,, \tag{6}$$

where $\mathbf{c}_e$ are the undetermined coefficients and $\dot{\mathbf{v}}_e$ and $\mathbf{N}_e$ are the particular and homogeneous solutions to governing equation (4), respectively such that

$$\mathcal{L}(\dot{\mathbf{v}}_e) = \overline{\mathbf{b}} \qquad \text{and} \qquad \mathcal{L}(\mathbf{N}_e) = 0 \qquad \text{on} \qquad \Omega_e \,. \tag{7}$$

The boundary tractions along the element boundary are derived from the Trefftz functions as

$$\mathbf{t}_e = \overset{\circ}{t}_e + \sum_{j=1}^{m} T_{ej} c_{ej} = \overset{\circ}{t}_e + \mathbf{T}_e \mathbf{c}_e \,, \tag{8}$$

where $\overset{\circ}{t}_e$ corresponds to $\overset{\circ}{v}_e$. The frame displacements

$$\tilde{\mathbf{u}} = \sum_e \sum_{i=1}^{N} \tilde{N}_{ei} d_{ei} = \sum_e \tilde{\mathbf{N}}_e \mathbf{d}_e \tag{9}$$

at the boundary Γ_e of a particular element are defined in the customary way in terms of nodal parameters $\mathbf{d}_e$ and, as in the conventional finite element formulation, satisfy the boundary conditions along Γ_{eu}. The element parameters $\mathbf{c}_e$ can be expressed in terms of nodal parameters $\mathbf{d}_e$ from (5b) as

$$\mathbf{c}_e = \mathbf{H}_e^{-1} \mathbf{G}_e \mathbf{d}_e - \mathbf{H}_e^{-1} \mathbf{h}_e \tag{10}$$

and from (5a) the element stiffness matrix $\mathbf{K}_e$ and the equivalent nodal forces $\mathbf{r}_e$ are

$$\mathbf{K}_e^T = \mathbf{G}_e^T \mathbf{H}_e \mathbf{G} \,, \qquad \mathbf{r}_e = \mathbf{g}_e - \mathbf{G}_e^T \mathbf{H}_e^{-1} \mathbf{h}_e \,, \tag{11}$$

where the auxiliary matrices are evaluated as the following integrals:

$$\mathbf{H}_e = \oint_{\Gamma_e} \mathbf{T}_e^T \mathbf{N}_e d\Gamma, \qquad \mathbf{G}_e = \oint_{\Gamma_e} \mathbf{T}_e^T \tilde{\mathbf{N}}_e d\Gamma,$$

$$\mathbf{h}_e = \oint_{\Gamma_e} \mathbf{T}_e^T \overset{\circ}{v}_e d\Gamma, \qquad \mathbf{g}_e = \oint_{\Gamma_e} \tilde{\mathbf{N}}_e^T (\overset{\circ}{t}_e - \bar{\mathbf{t}}_e) d\Gamma. \tag{12}$$

As may be seen, the evaluation of these element matrices only calls for integration along the element boundaries which permits to generate elements of a very general shape. Here it is worth mentioning that the symmetric property of $\mathbf{K}_e$ follows from the symmetry of matrix $\mathbf{H}_e$ which is, however, consequence of the energy consistent formulation of the basic differential equation (4). Since the final unknowns are the nodal degrees of freedom $\mathbf{d}_e$ and the formulation yields a symmetric positive definite stiffness matrix $\mathbf{K}_e$ this element is suitable for implementation to standard finite element programs.

Shell Element

The geometry for an arbitrary shell element is shown on *Fig. 1* where X, Y, Z are the global coordinates and x', y', z' are the C local ones. The element reference plane is defined by these x' and y' axes, while x and y are the orthogonal curvilinear surface coordinates lying along the midsurface principal curvature directions. For the size of elements normally used in finite element analysis of shells, the height z' above the reference plane is a small value. Hence, each element may be considered as geometrically shallow with respect to its own x' y' plane. This assumption is adopted exclusively to the geometry, and independently of this fact, both the deep or shallow shell theory can be implemented.

For geometrically shallow shell elements with any (more than five) nodes we may use a quadratic polynomial in the reference frame to interpolate the middle surface. Replacement of the actual middle surface by its osculating paraboloid permits to find the x, y directions of principal curvatures and the assumed, approximately constant $g_x = 1/R_x$, $g_y = 1/R_y$ values of principal curvatures. The sign of curvature is positive if the center point is located on the positive side of z direction. Furthermore, $(\partial z'/\partial x')^2 \ll 1$. $(\partial z'/\partial x')^2 \ll 1$ implies that the orthogonal axes x' and y' of the reference frame and the x and y projections will be parallel.

To develop an HT shell element, the choice of a suitable shell theory must first be made. Adopting the usual postulates of the first order theory of thin shells, the rotations and the nonvanishing strains in the x, y surface frame of the geometrically shallow element are given by [9] as:

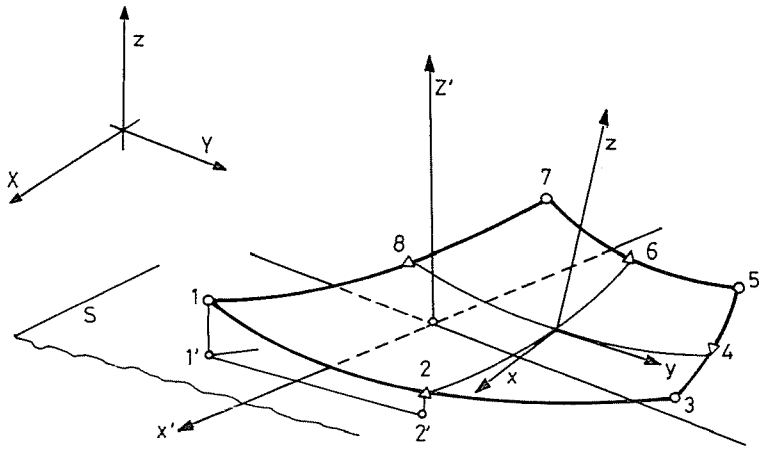

Fig. 1. Geometry and co-ordinate systems for geometrically shallow formulation

$$\alpha = \frac{\partial w}{\partial y} + \underline{g_y v}\,, \qquad \beta = -\frac{\partial w}{\partial x} - \underline{g_y u} \tag{13}$$

and

$$\varepsilon_x = \frac{\partial u}{\partial x} - g_x w + z \cdot \frac{\partial \beta}{\partial x}\,, \qquad \varepsilon_y = \frac{\partial v}{\partial y} - g_y w - z \cdot \frac{\partial \alpha}{\partial y}\,,$$

$$\varepsilon_{xy} = \frac{1}{2} \cdot \left(\frac{\partial v}{\partial x} + \frac{\partial u}{\partial y}\right) + z \cdot \frac{1}{2} \cdot \left(\frac{\partial \beta}{\partial y} - \frac{\partial \alpha}{\partial x}\right). \tag{14}$$

One may derive the five equations of equilibrium of thin shells with symmetric stress resultants and couples from the principle of virtual work which leads to the following energetically consistent description in the form

$$\frac{\partial N_x}{\partial x} + \frac{\partial N_{xy}}{\partial y} - \underline{g_x Q_x} = -p_x\,,$$

$$\frac{\partial N_y}{\partial y} + \frac{\partial N_{xy}}{\partial x} - \underline{g_y Q_y} = -p_y\,,$$

$$g_x N_x + g_y N_y + \frac{\partial Q_x}{\partial x} + \frac{\partial Q_y}{\partial y} = -p_z\,, \tag{15}$$

and the definition of transversal shear

$$Q_x = \frac{\partial M_x}{\partial x} + \frac{\partial M_{xy}}{\partial y},$$

$$Q_y = \frac{\partial M_y}{\partial y} + \frac{\partial M_{xy}}{\partial x}, \tag{16}$$

with the proper boundary conditions. Combination of the constitutive equations of one isotropic layer with the *Eqs.* (13–15) yields the following three governing differential equations in terms of the local displacements u, v, w which provide a suitable basis of a general HT thin shell element:

$$\left(1 + \underline{\frac{h^2}{12} \cdot g_x^2}\right) \cdot \left(\frac{\partial^2 u}{\partial x^2} + \frac{1-\nu}{2} \cdot \frac{\partial^2 u}{\partial y^2}\right) + \left(1 + \underline{\frac{h^2}{12} \cdot g_x g_y}\right) \cdot \frac{1+\nu}{2} \frac{\partial^2 v}{\partial x \partial y}$$

$$-(g_x + \nu g_y) \cdot \frac{\partial w}{\partial x} + \underline{\frac{h^2}{12} \cdot g_x \cdot \frac{\partial(\Delta w)}{\partial x}} = -\frac{p_x}{K},$$

$$\left(1 + \underline{\frac{h^2}{12} \cdot g_y^2}\right) \cdot \left(\frac{\partial^2 v}{\partial y^2} + \frac{1-\nu}{2} \cdot \frac{\partial^2 v}{\partial x^2}\right) + \left(1 + \underline{\frac{h^2}{12} \cdot g_x g_y}\right) \cdot \frac{1+\nu}{2} \frac{\partial^2 u}{\partial x \partial y}$$

$$-(g_y + \nu g_x) \cdot \frac{\partial w}{\partial y} + \underline{\frac{h^2}{12} \cdot g_y \cdot \frac{\partial(\Delta w)}{\partial y}} = -\frac{p_y}{K},$$

$$-(g_x + \nu g_y) \cdot \frac{\partial u}{\partial x} - (g_y + \nu g_x) \cdot \frac{\partial v}{\partial y} + (g_x^2 + g_y^2 + 2\nu g_x g_y) \cdot w$$

$$-\frac{h^2}{12} \cdot \underline{\left[\Delta \Delta w + g_x \cdot \frac{\partial(\Delta w)}{\partial x} + g_y \cdot \frac{\partial(\Delta w)}{\partial y}\right]} = -\frac{p_z}{K}. \tag{17}$$

Here

$$K = \frac{Eh}{1-\nu^2},$$

and Δ is the harmonic operator in the x, y surface frame of the geometrically shallow surface. The energy consistency here is reflected in the symmetry properties of differential operators [10–11]. However, this set of equations contains a number of terms which, in certain cases, are of small importance for the numerical results. To preserve the energy consistency

of the basic equations, simplifications can be made on the kinematic equations (13–14) only. The usual way is to ignore the underlined terms in *Eq.* (*13*) set

$$\alpha = \frac{\partial w}{\partial y}, \qquad \beta = -\frac{\partial w}{\partial x}. \tag{18}$$

This is equivalent to neglecting the contribution of the circumferential displacements u, v in the expressions of the bending strains. From the principle of virtual works, the consistent simplified equations of equilibrium may be shown to be represented by the *Eq.* (15) without the underlined shear force terms. Thus, the discarding of the $g_x Q_x$ and $g_y Q_y$ terms goes along with omission $g_x v$ and $g_y u$ in (13) whereas their separate handling would lead to shell theories unsuitable for the use in HT context. In deep structures these terms can be bypassed in axisymmetrical problems where $g_x v = g_y u = 0$. In other cases, we have to accept that the net finite element result converges toward the Donnel–Vlasov solution and expect the convergence toward the deep shell solution simply because the individual finite elements of a deep shell are geometrically shallow is irrelevant. A detailed discussion of the possible errors introduced by this step is found in [9]. Apart from some special situations — for example the simple bending of a circular cantilever — the numerical difference between the deep and shallow solutions is small, smaller than the numerical error coming from the discretization in many published reference results.

Combining the simplified equations (13) and (15) with the constitutive equations leads to *Eq.* (17) without the underlined terms. The energy consistency is reflected again in the preserved symmetry properties of differential operators.

The Trefftz functions $\overset{\circ}{v}_e$ and $\mathbf{N}_e$ can be generated as a particular solution and a T–complete set of homogeneous solution of the simplified *Eq.* (17). Next, we consider the homogeneous Fourier series solution for doubly curved shell of the form

$$\mathbf{v}_e = \begin{bmatrix} u \\ v \\ w \end{bmatrix} = \begin{bmatrix} U_{01}(x) \\ V_{01}(x) \\ W_{01}(x) \end{bmatrix} + \begin{bmatrix} U_{02}(y) \\ V_{02}(y) \\ W_{02}(y) \end{bmatrix} + \sum_n \left(\begin{bmatrix} U_{1n}(x)\cos(\alpha_y y) \\ V_{1n}(x)\sin(\alpha_y y) \\ W_{1n}(x)\cos(\alpha_y y) \end{bmatrix} \right.$$

$$\left. + \begin{bmatrix} U_{2n}(y)\sin(\alpha_x x) \\ V_{2n}(y)\cos(\alpha_x x) \\ W_{2n}(y)\cos(\alpha_x x) \end{bmatrix} + \begin{bmatrix} U_{3n}(x)\sin(\alpha_y y) \\ V_{3n}(x)\cos(\alpha_y y) \\ W_{3n}(x)\cos(\alpha_y y) \end{bmatrix} + \begin{bmatrix} U_{4n}(y)\cos(\alpha_x x) \\ V_{4n}(y)\sin(\alpha_x x) \\ W_{4n}(y)\sin(\alpha_x x) \end{bmatrix} \right) \tag{19}$$

with

$$\alpha_x = \frac{n\pi}{l_x}, \qquad \alpha_y = \frac{n\pi}{l_y}, \tag{20}$$

where l_x and l_y are suitably, chosen dimensions. Presently, $l_x = l_y =$ radius of circumscribing circle and the $x = y = 0$ origin is placed in the center of element. Introducing this series into (17) and setting $p_x = p_y = p_z = 0$ leads to a system of ordinary differential equations for the unknown functions U, V, W which can be easily solved [16]. The usual procedure leads to polynomials with eight complex roots, thus, each (U_{in}, V_{in}, W_{in}) set in (19) includes eigth independent components and, as a consequence, there are 32 independent solutions to *Eq.* (5) for each $n > 1$. The $n = 0$ solution can be composed of $4+4 = 8$ independent functions. From these solutions we may construct the in-element matrices of the HT shell element, namely the generalized displacements (6), internal forces and internal traction fields (8) as

$$\mathbf{v}_e^T = [u, v, w, \alpha, \beta],$$
$$\boldsymbol{\sigma}_e^T = [N_x, N_y, N_{xy}, Q_x, Q_y, M_x, M_y, M_{xy}],$$

$$\mathbf{t}_e = \begin{bmatrix} N_{nx} \\ N_{ny} \\ Q_n \\ M_{nx} \\ M_{ny} \end{bmatrix} = \begin{bmatrix} N_x n_x + N_{xy} n_y \\ N_{xy} n_x + N_y n_y \\ Q_x n_x + Q_y n_y \\ -M_{xy} n_x + M_x n_y \\ M_x n_x + M_{xy} n_y \end{bmatrix}, \tag{21}$$

with components in local x, y surface frame.

The interelement continuity and the boundary conditions are enforced via the interelement field or frame functions which are defined in terms of the five conventional nodal parameters $[u, v, w, \alpha, \beta]$ of thin shell elements. Because the Kirchhoff assumption is used, the $\tilde{\mathbf{u}}$ frame function (9) should include suitable and independent interpolations of $\tilde{u}$, $\tilde{v}$, $\tilde{w}$ displacements and the normal rotation $\tilde{w}_n = \partial\tilde{w}/\partial n$.

For the *p*–version of HT element, in addition to the linear interpolation of $\tilde{u}$, $\tilde{v}$, $\tilde{w}_n$ and the cubic interpolation of transverse displacement $\tilde{w}$, the $\tilde{u}$ frame function will be supplemented with optional number M of hierarchic modes along each element side. With the notation of *Fig. 2,* such frame functions along the element side A–C–B can be defined as

$$\tilde{u} = \tilde{u}_A N_1(\xi) + \tilde{u}_B N_2(\xi) + \sum a_i L_i(\xi) S^{i-1},$$

$$\tilde{v} = \tilde{v}_A N_1(\xi) + \tilde{v}_B N_2(\xi) + \sum b_i L_i(\xi) S^{i-1},$$

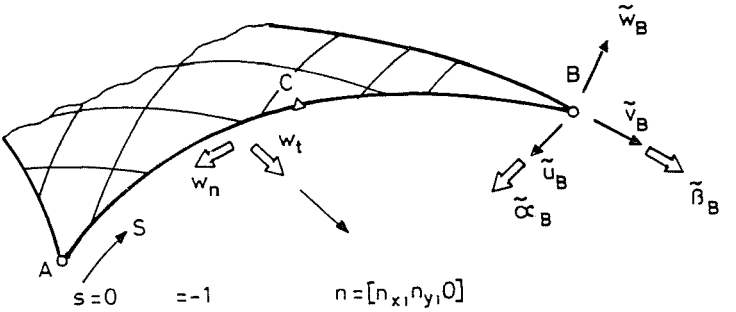

Fig. 2. Displacements and rotations of the frame

$$\tilde{w}_n = \tilde{w}_{nA} N_1(\xi) + \tilde{w}_{nB} N_2(\xi) + \sum c_i L_i(\xi) S^i ,$$

$$\tilde{w} = \tilde{w}_A N_3(\xi) + \tilde{w}_{tA} J N_4(\xi) + \tilde{w}_B N_5(\xi) + \tilde{w}_{tB} J N_6(\xi) + \sum d_i M_i(\xi) S^{i-1} . \quad (22)$$

Here $J = |ds/d\xi|$, $-1 \leq \xi \geq +1$, and the Hermitean shape functions and the bubble functions are [5]

$$N_1 = (1-\xi)/2 , \qquad N_2 = (1+\xi)/2 ,$$
$$N_3 = (\xi^3 - 3\xi + 2)/4 , \qquad N_4 = (\xi^3 - \xi^2 - \xi + 1)/4 ,$$
$$N_5 = (-\xi^3 + 3\xi + 2)/4 , \qquad N_6 = (\xi^3 + \xi^2 - \xi - 1)/4 ,$$
$$L_i = \xi^{i-1}(1-\xi^2) , \qquad M_i = \xi^{i-1}(1-\xi^2)^2 , \qquad i = 1, 2, \ldots .$$

The value of coefficient S in (22) is equal either to $+1$ or -1 according to the orientation of A–C–B side.

The purpose of S is to ensure the unic displacement definition for even and odd bubble functions along A–C–B line common to two element sides with opposite orientation. The final matrix form of frame functions for a particular element side in terms of nodal parameters, using the simple transformation of rotations on *Fig. 3* as

$$\tilde{\alpha} = \tilde{w}_t n_x + \tilde{w}_n n_y , \qquad \beta = \tilde{w}_t n_y - \tilde{w}_n n_x ,$$

$$w_t = \frac{1}{J} \cdot \frac{\partial w}{\partial \xi} ,$$

may now be written as

$$\tilde{\mathbf{u}} = \begin{bmatrix} \tilde{u} \\ \tilde{v} \\ \tilde{w} \\ \tilde{\alpha} \\ \tilde{\beta} \end{bmatrix} = \tilde{\mathbf{N}}_{\mathrm{As}} \cdot \begin{bmatrix} \tilde{u} \\ \tilde{v} \\ \tilde{w} \\ \tilde{\alpha} \\ \tilde{\beta} \end{bmatrix}_{\mathrm{A}} + \tilde{\mathbf{N}}_{\mathrm{Bs}} \cdot \begin{bmatrix} \tilde{u} \\ \tilde{v} \\ \tilde{w} \\ \tilde{\alpha} \\ \tilde{\beta} \end{bmatrix}_{\mathrm{B}} + \tilde{\mathbf{N}}_{\mathrm{Cs}} \cdot \begin{bmatrix} a_1 \\ b_1 \\ c_1 \\ d_1 \\ a_2 \\ b_2 \\ \cdot \\ \cdot \\ \cdot \end{bmatrix}, \qquad (23)$$

where the submatrices are as follows:

$$\underset{(5\times 5)}{\tilde{\mathbf{N}}_{\mathrm{As}}} = \begin{bmatrix} N_1 & 0 & 0 & 0 & 0 \\ 0 & N_1 & 0 & 0 & 0 \\ 0 & 0 & N_3 & Jn_{\mathrm{x}}N_4 & Jn_{\mathrm{y}}N_4 \\ 0 & 0 & n_{\mathrm{x}}N_3'/J & n_{\mathrm{x}}^2N_4' + n_{\mathrm{y}}^2N_1 & n_{\mathrm{x}}n_{\mathrm{y}}(N_4' - N_1) \\ 0 & 0 & n_{\mathrm{y}}N_3'/J & n_{\mathrm{x}}n_{\mathrm{y}}(N_4' - N_1) & n_{\mathrm{y}}^2N_4' + n_{\mathrm{x}}^2N_1 \end{bmatrix},$$

$$\underset{(5\times 5)}{\tilde{\mathbf{N}}_{\mathrm{Bs}}} = \begin{bmatrix} N_2 & 0 & 0 & 0 & 0 \\ 0 & N_2 & 0 & 0 & 0 \\ 0 & 0 & N_5 & Jn_{\mathrm{x}}N_6 & Jn_{\mathrm{y}}N_6 \\ 0 & 0 & n_{\mathrm{x}}N_5'/J & n_{\mathrm{x}}^2N_6' + n_{\mathrm{y}}^2N_2 & n_{\mathrm{x}}n_{\mathrm{y}}(N_6' - N_2) \\ 0 & 0 & n_{\mathrm{y}}N_5'/J & n_{\mathrm{x}}n_{\mathrm{y}}(N_6' - N_2) & n_{\mathrm{y}}^2N_6' + n_{\mathrm{x}}^2N_2 \end{bmatrix},$$

$$\underset{(5\times \mathrm{M})}{\tilde{\mathbf{N}}_{\mathrm{Cs}}} = \begin{bmatrix} L_1 & 0 & 0 & 0 & L_2S & 0 & 0 \\ 0 & L_1 & 0 & 0 & 0 & L_2S & 0 \\ 0 & 0 & 0 & M_1 & 0 & 0 & 0 \\ 0 & 0 & n_{\mathrm{y}}L_1S & n_{\mathrm{x}}M_1'/J & 0 & 0 & n_{\mathrm{y}}L_2 \\ 0 & 0 & -n_{\mathrm{x}}L_1S & n_{\mathrm{y}}M_1'/J & 0 & 0 & -n_{\mathrm{x}}L_2S \end{bmatrix}$$

$$\begin{bmatrix} 0 & L_3 & 0 & 0 & 0 & \dots \\ 0 & 0 & L_3 & 0 & 0 & \\ M_2S & 0 & 0 & 0 & M_3 & \\ n_{\mathrm{x}}M_2'S/J & 0 & 0 & n_{\mathrm{y}}L_3S & n_{\mathrm{x}}M_3'/J & \\ n_{\mathrm{y}}M_2'S/J & 0 & 0 & -n_{\mathrm{x}}L_3S & n_{\mathrm{y}}M_3'/J & \end{bmatrix}. \qquad (24)$$

The M hierarchic degrees of freedom of an element side can be associated with its mid-side node C (see *Fig. 2*). In the p version, the solution accuracy

is controlled by modifying uniformly or selectively these side freedoms M while the mesh remains fixed. The increase of M numbers is accompanied by corresponding increase of m, the number of Trefftz functions in (20). The necessary but not sufficient condition for the stiffness matrix to be of correct rank is

$$m \geq \text{NDOF} - \text{NRIG}, \tag{25}$$

where NDOF is the number of element degrees of freedom (vector $\mathbf{d}_e$) and NRIG= 6 the number of rigid body modes. The numbers m given in *Table 1* have been chosen to satisfy the stability condition (25) and provide a direction insensitive displacement field.

Table 1
Numbers m and M of Trefftz and frame functions.
NG: Gauss points per side, DOF: total element freedoms

M	Triangl.		Quadr.		NG
	m	DOF	m	DOF	
0	24	15	24	20	8
3	24	24	40	32	8
7	40	36	56	48	10
11	56	48	72	64	12
15	72	60	88	80	14

It is obvious from the definition (12) of the matrices $\mathbf{H}_e$ and $\mathbf{G}_e$ that the $\mathbf{v}_e$ must not include the zero strain displacement terms. These missing $\mathbf{v}_{Re}$ terms, if necessary, can be calculated later by the least square matching between the nodal values of (6) and the functions (9) as

$$\sum_i \left(\mathbf{v}_e + \mathbf{v}_{Re} - \tilde{\mathbf{N}}_e \mathbf{d}_e\right)^2 = \text{minimum}. \tag{26}$$

The $\mathbf{v}_{Re}$ zero strain displacement mode of the Donnel – Vlasov theory is given as

$$\mathbf{v}_{Re} = \begin{bmatrix} u_R \\ v_R \\ w_R \\ \alpha_R \\ \beta_R \end{bmatrix} = a_1 \cdot \begin{bmatrix} 1 \\ 0 \\ 0 \\ 0 \\ 0 \end{bmatrix} + a_2 \cdot \begin{bmatrix} 0 \\ 1 \\ 0 \\ 0 \\ 0 \end{bmatrix} + a_3 \cdot \begin{bmatrix} g_x x \\ g_y y \\ 1 \\ 0 \\ 0 \end{bmatrix}$$

$$+a_4 \cdot \begin{bmatrix} (g_y y^2 - g_x x^2)/2 \\ -g_y xy \\ -x \\ 0 \\ 1 \end{bmatrix} + a_5 \cdot \begin{bmatrix} g_x xy \\ (g_y y^2 - g_x x^2)/2 \\ y \\ 1 \\ 0 \end{bmatrix} + a_6 \cdot \begin{bmatrix} -y \\ x \\ 0 \\ 0 \\ 0 \end{bmatrix} . \quad (27)$$

Numerical Study

The quadrilateral HT shell element was implemented and tested in a finite element program system and its performance was assessed on the following two examples:

A. The problem of a short circular cylinder with an axisymmetric line load serves as a good tool to analyse the capacity of the HT element to represent highly localized effects (*Fig. 3*). Because of the symmetry, only a segment was analysed with local displacements and rotations. The nodal loads $\mathbf{r}_e$ (11) were calculated as the usual work equivalents, just as $\dot{\mathbf{t}}_e = 0$, $\dot{\mathbf{v}}_e = 0$. The results in *Table 2* show the rapid convergence of the peak bending moment with increasing M side DOF, and a slightly slower convergence with increasing number of elements along the generator. The difference in bending moments M_x at points A and C of *Fig. 3* shows that the axisymmetric behaviour of Trefftz functions — which was imposed via the boundary conditions — is recovered with higher M values only. It is due to the fact that the polynomial frame functions of lower degree could not enforce the rapidly varying exponential distribution on the internal field which otherwise includes the necessary components of the theoretically exact solution. This fact can be observed on the results in *Table 3* as well where a selective control of p method was used by changing the numbers of freedoms at side nodes C and S independently. The results for the deflection are much more accurate than the internal forces. For example, with a single element used with $M = 0$ at all sides, the deflection $w_A = 0.69904$ is less than 1% in error with respect to the exact 0.70612 value. The error distribution study showed that the errors are the largest always at the element corner.

B. Pinched cylinder with end diaphragms (*Fig. 4*). This example was used to test the element ability to model both inextensional bending and complex membrane states. The reference deflection $w_C = -1.825 \cdot 10^{-5}$ [4] under the load was computed from Fourier series expansion of Flügge's deep cylindrical shell equation. The deflection results summarized in *Table 4* show convergence toward the

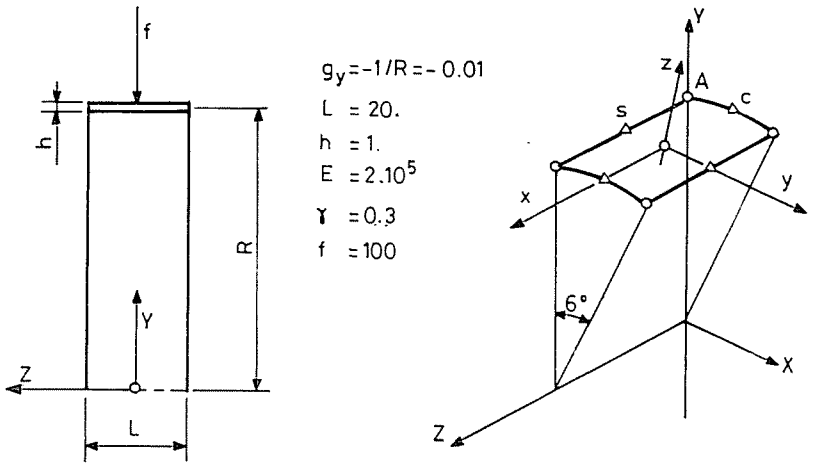

Fig. 3. Short cylinder with axisymmetric line load

Table 2
Short axisymmetric cylinder, % errors in moment M_x at C and A and in shear force Q_x at C. Exact resulte $M_{xA} = M_{xA} = -409.848$, $Q_x = 100.0$.

M	1×1			1×2			1×3		
	ΔM_{xC}	ΔM_{xA}	ΔQ_{xC}	ΔM_{xC}	ΔM_{xA}	ΔQ_{xC}	ΔM_{xC}	ΔM_{xA}	ΔQ_{xC}
0	-8.41	21.90	-7.62	0.76	-5.17	4.72	0.44	-0.98	2.10
3	-5.23	20.29	-1.89	0.73	-4.74	4.42	0.43	-0.91	2.00
7	0.42	-1.57	2.05	0.03	-0.02	0.16	0.	0.	0.02
11	-0.01	0.14	0.01	0.	0.	0.02	0.	0.	0.
15	0.	0.	0.03	0.	0.	0.	0.	0.	0.

$\tilde{w}_C = w_C = -1.793 \cdot 10^{-5}$ which is the converged shallow shell solution of this problem. The difference between the two theories is less than 1.5% in this value. It is worth mentioning that the difference between Trefftz deflection w_C (20) modified with the zero strain displacement (27) and frame (nodal) deflection $\tilde{w}_C$ (23) appears to be proportional to the accuracy. In *Table 5*, the internal force components at point A can be seen. The rate of convergence is slower in this point which is close to the location of singularity. In the presented form, the P force was taken into account as a work equivalent nodal load. According to the experience with the HT plate element, the accuracy can increase if the given loads are incorporated via the $\dot{\mathbf{v}}_e$

Table 3

Short axisymmetric cylinder. Selective p–convergence for 1×1 mesh. % error in M_{xA}. MS=hierarchic DOF at straight sides. MC=hierarchic DOF at curved sides, total number of DOF in brackets

	MS			
MC	3	7	11	15
0	-20.29 (26)	-1.53 (34)	-0.01 (42)	0. (50)
3	-20.29 (32)	-1.53 (40)	-0.01 (42)	0. (56)
7	-24.90 (40)	-1.57 (48)	0.01 (56)	0. (64)
11	-25.75 (48)	-1.71 (56)	0.14 (64)	0. (72)
15	-27.62 (56)	-1.75 (64)	0.16 (72)	0. (80)

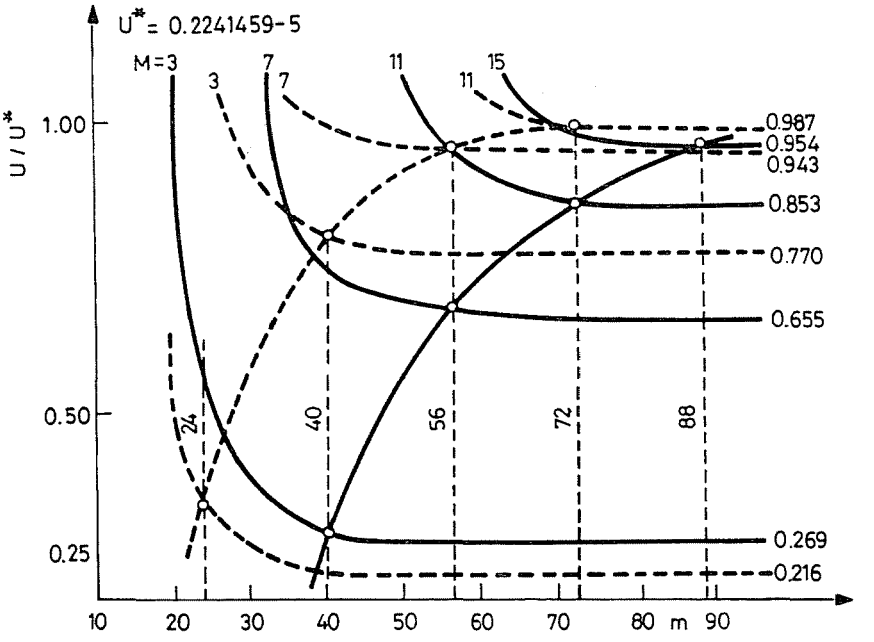

Fig. 4. Pinched cylinder with end diaphragms. Boundary conditions $x = L/2$, $\tilde{v} = \tilde{w} = \alpha = 0$

particular solution. This can be done by adopting the fundamental solution given in [15].

Because of its complexity, this example is useful to study the optimal number of trial functions. If the m number of internal functions in (6) or in (20) is high relative to the M side degrees of freedom in (24) (number of frame functions), this may lead to unefficient overdimensioning in the

Table 4
Pinched cylinder with end diaphragm,
p and h convergence of deflection under the load from internal/frame field,
DOF in brackets. Solution *: $m = 104$.

M	$-w_c \cdot 10^5 / -\bar{w}_c \cdot 10^5$			
	1×1		2×2	
0	0.0482/0.0744	(20)	0.1355/0.1818	(45)
3	0.1211/0.1095	(32)	0.5143/0.5256	(81)
7	0.4427/0.4645	(40)	1.2221/1.2175	(129)
11	0.9672/0.9297	(48)	1.5571/1.5389	(177)
15	1.2678/1.3025	(56)	1.7183/1.7169	(225)
	4×4		8×8	
0	0.4391/0.6035	(125)	1.1651/1.4471	(405)
3	1.3938/1.4328	(245)	1.6967/1.7305	(837)
7	1.6970/1.7096	(405)	1.7809/1.7877	(1413)
11	1.7739/1.7733	(565)	1.7918/1.7937	(1989)
15	1.7864/1.7863	(725)	1.7918/1.7920	(2565)
	16×16			
0	1.6509/1.7416	(1445)		
3	1.8152/1.8289	(3077)		
7	1.7980/1.8003	(5253)		
11	1.7983/1.7999	(7429)		
15	1.7934/1.7935	(9605)		
15*	1.7931/1.7931	(9605)		

Table 5
Pinched cylinder with end diaphragm.
Internal forces at point A of *Fig. 4*

M	$-M_{yA} \cdot 10^{-1}$			
	2×2	4×4	8×8	16×16
0	0.028	0.147	0.856	1.560
3	0.198	0.830	1.442	1.551
7	0.502	1.179	1.359	1.233
11	0.971	1.350	1.210	1.231
15	1.141	1.308	1.229	1.250
	$-N_{xA} \cdot 10^{-2}$			
0	0.257	0.529	0.759	5.855
3	0.963	3.367	5.251	4.861
7	3.794	4.470	4.768	4.772
11	4.703	5.152	4.821	5.071
15	4.980	5.011	4.955	4.990

assembled problem. To illustrate the nature of convergence, *Fig. 5* displays for 2×2 and 4×4 meshes the change of normalized strain energy U/U^*. (Here $U^* = 0.2241459 \cdot 10^{-5}$ calculated on 16×16 mesh with $M = 15$ and $m = 104$). This figure clearly shows the convergence for fixed M and m (h–convergence) and for fixed mesh and M (p–convergence). In the latter case, the stabilized final value highly depends on the M number of side modes in the frame field. In other words, these stabilized solutions are referred to the given structure constrained by the 'weak' polynomial frame functions. This result confirms the data of *Table 1* which indicates the combined increase of m and M.

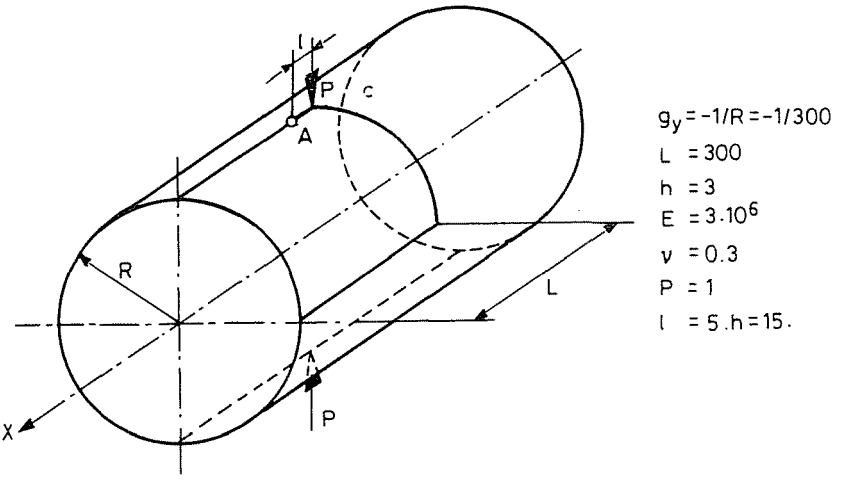

Fig. 5. Pinched cylinder with end diaphragms. Convergence and optimum M–m analysis for 2×2 (continuous line) and 4×4 (dashed line) meshes

The trend of research is presently to implement the solution of the more general basic equation (17) and to extend the formulation relying on the observations of the successful HT plate bending elements [3–6].

Concluding Remarks

The study has demonstrated the possibility of extension of the HT FE model to thin shells. Although the Trefftz functions used here have been based on a shallow shell theory, the deep shell theory can also be used. Provided that the coefficients of the governing differential equations remain constant and, as a consequence, the principal curvatures of the middle

surface do not vary over the element, the generation of such functions presents no basic problem. The requirement of constant curvatures implies that shells of a general geometry will have to be approached by using comparatively small h-method HT elements rather than the large HT p-elements the use of which will be confined to special forms of shell geometry and load cases. The Trefftz functions used in the present study represent only one of possible choices. A considerable amount of further research will be necessary before the HT shell elements reach a degree of maturity comparable to that now achieved by the HT plate and plane elasticity elements.

Acknowledgements

This research was supported by 'Schweizerischer Nationalfonds zur Förderung der wissenschaftlichen Forschung'. The author gratefully acknowledges the discussions with Prof. J.Jirousek in Lausanne.

References

1. FLÜGGE, W.: Stresses in Shells, Springer-Verlag, 1960.
2. KRAUS, H.: Thin Elastic Shells, John Wiley, 1967.
3. TONG, P.: New Displacement Hybrid Finite Element Model for Solid Continua, *Int. J. Numer. Methods Eng.*, Vol. 2, pp. 73–83 (1970).
4. RUOFF, G.: Die praktische Berechnung der Kopplungsmatrizen bei der Kombination der Trefftzschen Methode und der Methode der finite Elemente, in Finite Elemente in der Statik, Ernst, Berlin, 1973.
5. GALLAGHER, O. C.: Finite Element Analysis: Fundamentals, Englewood Cliffs, N. J. Prentice-Hall, 1975.
6. MORRIS, A. J.: A Summary of Appropriate Governing Equations and Functionals in the Finite Element Analysis of Thin Shells, in Finite Elements for Thin Shells and Curved Members, ed. D. G. Ashwell and R. H. Gallagher, John Wiley, 1976.
7. JIROUSEK, J. – LEON, N.: A Powerful Finite Element for Plate Bending, *Comp. Meth. Appl. Mech. Eng.* Vol. 12, pp. 77–96 (1977).
8. MATSUI, T. – MATSUOKA, O.: The Fundamental Solution in the Theory of Shallow Shells, *Int. J. Solids Structures*, Vol. 14, pp. 971–986 (1978).
9. KRATZIG, W. B.: On the Structure of Consistent Linear Shell Theories, in Proc. of 3rd IUTAM Symposium on Theory of Shells in Tbilisi, ed. W. T. Koiter and G. K. Mikhailov, North Holland, 1980.
10. JIROUSEK, J. – TEODORESCU, P.: Large Finite Element Method for the Solution of Problems in the Theory of Elasticity, *Computers and Structures*, Vol. 15, pp. 575–587 (1982).
11. JIROUSEK, J.: Structural Analysis Program SAFE–Special Features and Advanced Finite Element Models, *Adv. Eng. Software*, Vol. 7, pp. 68–76 (1985).
12. JIROUSEK, J. – GUEX, L.: The Hybrid-Trefftz Finite Element Model and its Application to Plate Bending, *Int. J. Numer. Methods Eng.*, Vol. 23, pp. 651–693 (1986).

13. VENKATESH, A. – JIROUSEK, J.: An Improved 9 DOF Hybrid-Trefftz Triangular Element for Plate Bending, *Engineering Computations*, Vol. 4, pp. 202–222 (1987).
14. JIROUSEK, J.: Hybrid-Trefftz Plate Bending Elements with p–method Capabilities, *Int. J. Numer. Methods Eng.* Vol. 24, pp. 1367–1393 (1987).
15. WHITE, D. W. – ABEL, J. F.: Testing of Shell Finite Element Accuracy and Robustness, *Finite Elements in Anal. and Design*, Vol. 6. pp. 129–151 (1989).
16. JIROUSEK, J. – VENKATESH, A.: A New FE Approach with Optimal Suitability for Adaptive Reliability Assurance, IREM Internal report 90/4, Ecole Polytechnique Fédérale de Lausanne, (1990).

Address:

Dr. Gábor VÖRÖS
Department of Technical Mechanics
Technical University of Budapest
H–1521 Budapest, Hungary